Engineering the Optoelectronic Properties of 2D Hexagonal Boron Nitride Monolayer Films by Sulfur Substitutional Doping

Biying Tan[1,2], You Wu[1,2], Feng Gao[2], Huihui Yang[2], Yunxia Hu[2], Huiming Shang[1,2], Xin Zhang[1,2], Jia Zhang[2], Zhonghua Li[1,2], Yong-Qing Fu[5], Dechang Jia[3], Yu Zhou[3], Haiying Xiao[3]* and PingAn Hu[1,2,3,4]*

[1] School of Chemistry and Chemical Engineering, Harbin Institute of Technology, Harbin 150080, P. R. China.
[2]Key Laboratory of Micro-Systems and Micro-Structures Manufacturing of Ministry of Education, Harbin Institute of Technology, Harbin 150080, P. R. China.
[3]School of Materials Science and Engineering, Harbin Institute of Technology, Harbin, 150080, P. R. China.
[4] State Key Laboratory of Robotics and Systems, Harbin Institute of Technology, Harbin 150080, P. R. China.
[5] Faculty of Engineering & Environment, Northumbria University, Newcastle uponTyne, NE1 8ST, UK.
Corresponding Authors: xhyhit@hit.edu.cn; hupa@hit.edu.cn

ABSTRACT: Tuning the optical and electrical properties of two-dimensional (2D) hexagonal boron nitride (hBN) is critical for its successful applications in optoelectronics. Herein, we report a new methodology to significantly enhance optoelectronic properties of hBN monolayer by substitutionally doped with sulfur (S) on a molten Au substrate using chemical vapor deposition. The S atoms are more geometrically and energetically favorable to be doped in N sites than in B sites of the hBN, and the S 3p orbitals hybridize with the B 2p orbitals, forming a new conduction band edge that narrows its bandgap. The band edge positions change with the doping concentration of S atoms. The conductivity increases up to 1.5 times and enhances the optoelectronic properties, compared to the pristine hBN. A photodetector made of the 2D S-doped hBN film shows an extended wavelength response from 260 nm to 280 nm, and a 50-times increase in its photocurrent and responsivity with the light illumination at 280 nm. These enhancements are mainly due to the improved light absorption and increased electrical conductivity through doping with sulfur. This S doped hBN monolayer film can be used as the next generation electronics, optoelectronics, and spintronics.

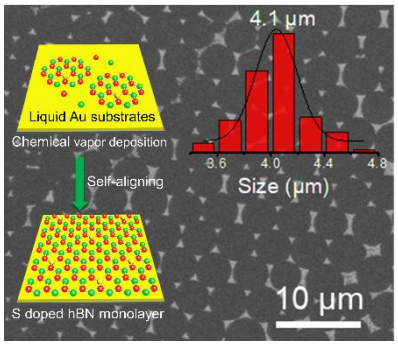

KEYWORDS: *hexagonal boron nitride, chemical vapor deposition, 2D monolayer films, sulfur substitutional doping, optoelectronic properties, deep UV photodetectors*

INTRODUCTION

Hexagonal boron nitride (hBN) is one of the key two-dimensional (2D) materials, composing of alternating B and N atoms bonded by strong sp^2 covalent bonds in its hexagonal lattices.[1] Due to its atomically flat structure, chemical stability and excellent dielectric property, the hBN has been extensively explored as substrates, passivation layers, gate dielectric and tunneling layers, etc., to construct 2D van der Waals heterostructures.[2-7] Recently, its single-photon emission, nonvolatile, piezoelectric and hyperbolic properties are investigated.[8-11] These intriguing electronic, optoelectronic and electromagnetic properties facilitate its practical uses in single-photon emitters, memristors, and hyperlenses.[8-13] However, due to its ultra-wide bandgap, hBN is unsuitable for many optoelectronic applications. For instance, the hBN is reported to have a low electrical conductivity and a weak light absorption capability with the wavelength longer than 260 nm, which results in relatively low responsivity and poor detectivity when utilized in deep ultraviolet photodetectors.[14-16] Therefore, modulating the optical and electrical properties of the hBN is critical for its applications in optoelectronics.[17-18]

Recently, great efforts have been made to effectively modify the properties of hBN by functionalizing it with terminating bonds, such as -H, -F, -OH, and -NH_2, and/or substitutionally doping with metal elements of Li, Be, Mg, Zn and nonmetal elements of C, O, and S.[19-26] Compared to the chemisorption methods using the functional groups, substitutionally doping in the host lattice is more stable and feasible. Especially, theoretical studies have revealed that substitutionally doping with sulfur resulted in remarkable modifications in electrical and optoelectrical properties of the hBN,[27,28] although there is no experimental study for the S substitutionally doped hBN monolayer. Xu and Wang groups have reported that the S doped hBN powders showed enhanced light absorption and charge transfer capabilities with excellent photocatalytic degradation of pollutants.[25, 26] However, it is a huge challenge to obtain large scale substitutionally doped 2D hBN film using the conventional chemical vapor deposition

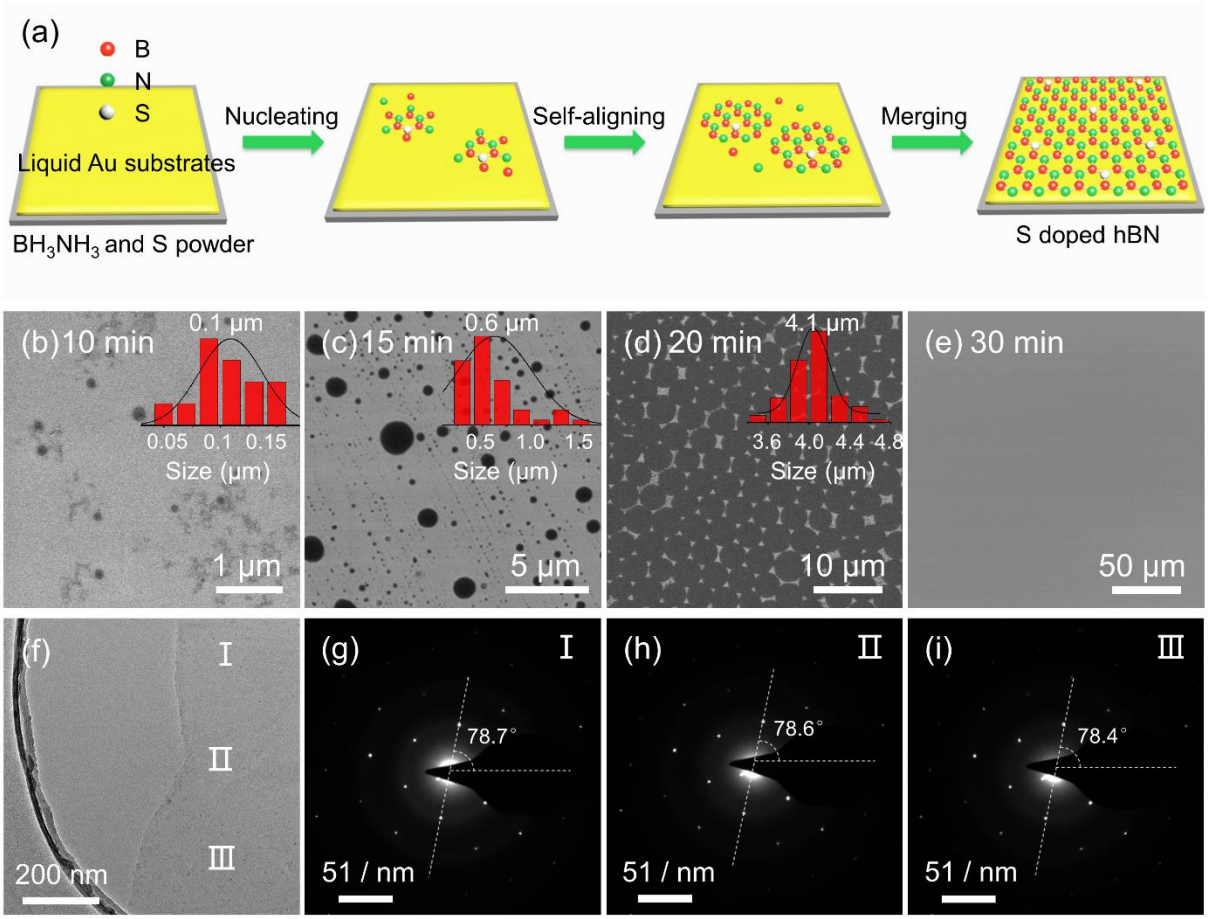

Figure 1. Aligned growth of S doped hBN monolayer film on a liquid Au layer. (a) Schematic illustration of aligned growth process of S doped hBN monolayer films. (b-e) SEM images of the growth process after 10 min, 15min, 20 min, 30 min, respectively. (f) TEM image of merging region of two domains. (g-i) SAED patterns of the corresponding marked areas in panel 1f.

(CVD). This is mainly due to the difficulty of substitutionally doping of S into the host lattice of hBN at a high temperature and various facile reactions occurred between the elemental S and commonly used metal foil (Cu, Ni, and their alloys, Pt substrates) during the CVD process. [29, 30]

In this work, we successfully prepare the S doped hBN monolayer films on molten Au substrates by ambient pressure chemical vapor deposition (APCVD), and then systematically study their optical and electrical properties. The doping concentrations of S atoms can be tuned from 0.3% to 0.9% without deteriorating the quality of host hBN films by precisely controlling the reagent sources of B, N and S. Both experiments and first-principles density functional theory (DFT) calculations manifest that the S dopants replace the N sites in the hexagonal lattices and form S-B bonds. The band edges are shifted downwards, and the bandgap is narrowed by 140 meV from 5.83 eV to 5.69 eV after S doping, which improves the electrical conductivity and extends the light response range up to a wavelength of 280 nm for a constructed photodetector. The strategy of S doped hBN monolayer films provides a new route to enhance the optoelectronic properties in the realm of 2D materials.

RESULTS AND DISCUSSION

Both S-free and S-doped hBN monolayer films were directly synthesized on a molten Au layer on a tungsten plate using APCVD. For the S-doped hBN, three representative doping concentrations of 0.3%, 0.6% and 0.9% (at. %) were obtained by mixing 1.0 mg, 2.0 mg and 3.0 mg of sulfur powders with 10.0 mg ammonia borane, respectively. We chose the Au layer for the growth of S doped hBN monolayer due to its good catalytic ability, low solubilities of B and N atoms for monolayer films synthesis, and a reasonable sulfur-resistant characteristics at a high temperature.[29-31] It has been reported that the shape of the synthesized domains is highly dependent on the ratio of B to N on the surface of substrates.[32] To obtain a circular single-crystal shape, the distances of B, N and S sources and the substrate were set to be 55 cm in a 1 inch quartz tube. Aligning growth of hBN domains is another common strategy to obtain wafer-scale single-crystal hBN films.[33-35] The self-alignment of circular domains follows the minimized energy principle during its growth at a high temperature. To avoid formation of energetically unfavorable grain boundaries, the adjacent domains could be precisely aligned with each other by

either rotating or translating before they are merged together.

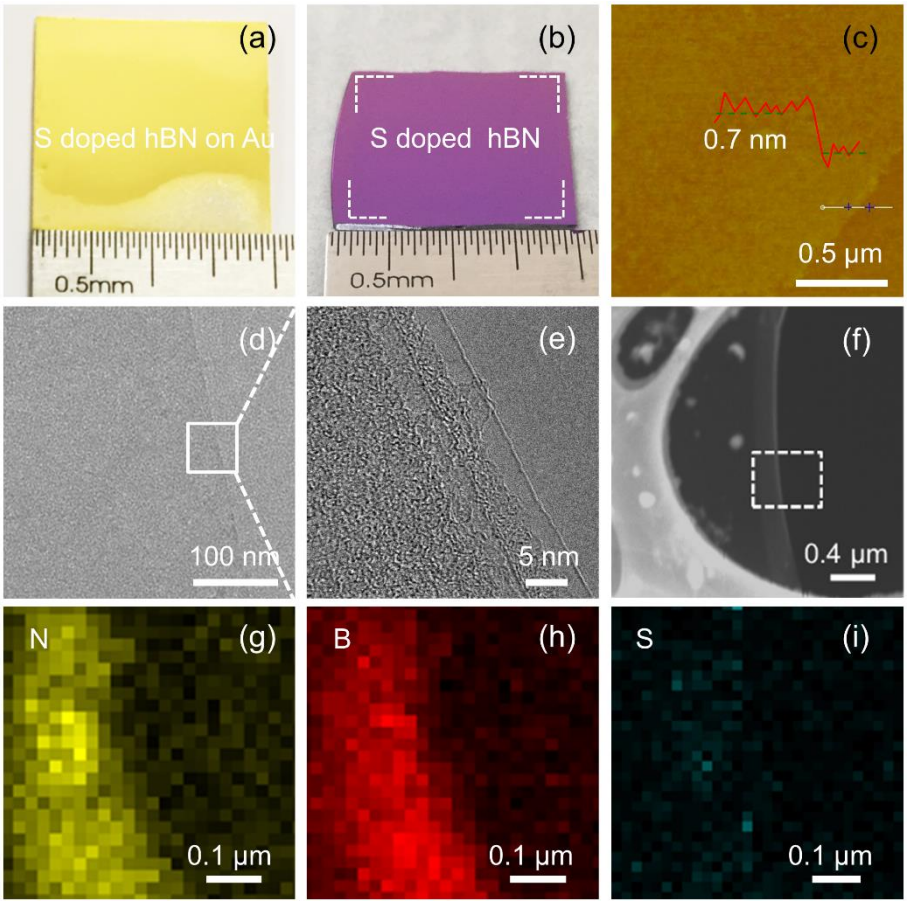

Figure 2. Monolayer film features and S doping characterizations. (a) Photograph of as-grown S doped hBN monolayer films on Au substrates. (b, c) Photograph and AFM image of S doped hBN monolayer films transferred onto SiO_2/Si substrates. (d, e) TEM images of S doped hBN monolayer films. (f) STEM image of the S doped hBN monolayer films. (g-i) EDS mappings of (g) N-K, (h) B-K, and (i) S-K, the inset in panel 2f showing the measured area.

Ideally, on the atomically smooth and quasi-diffusion barrier free liquid Au surface, both rotation and translation can happen simultaneously for these merging domains. We systematically studied the orientations of these domains by different characterization methods.

The substrate was pre-annealed at 1035 ℃ for 30 min to remove impurities which can reduce nucleation density and cause disordered nucleation. Then it was heated up to 1085 ℃ slowly (~5℃/min) to obtain a smooth and liquid Au surface on the tungsten plate. Figure 1a shows the schematic illustration of growth process for the S doped hBN monolayer film. After heating the reactant sources for 10 min, only a few circular domains started to nucleate (Figure 1b). The nucleation density and the domain size increased rapidly within 15 min (Figure 1c). These individual domains reached to a uniform size of about 4.1 μm determined by statistical analysis and nucleation was saturated at ~20 min (Figure 1d and Figure S1). Finally, more and more circular domains contacted and precisely aligned with each other guided by the electrostatic forces, and then coalesced to form a smooth and uniform monolayer film (Figure 1e). After the formation of S doped hBN, the Au surface was still smooth and shiny without deterioration caused by the sulfur atoms in the deposition chamber. To maintain smooth surfaces and avoid formation of any cracks or wrinkles, the furnace was cooled down to 1035 ℃ within 9 min and maintained for 10 min to solidify the molten Au substrates. The smooth surface of the substrate is essential for both the aligned growth and transfer of the S doped hBN (Figure S2). The homogeneous pink color in the inverse pole figure (IPF) maps of electron beam scattering diffraction (EBSD) patterns shown in Figure S3 indicates that the whole region of the Au substrate has a (001) facet after the cooling process.

Orientations of these domains were characterized using transmission electron microscope (TEM) combined with their selective area electron diffraction (SAED) patterns (Figure 1f-i). The TEM image of the merged region manifests the homogenous structure of the domains (Figure 1f). The SAED patterns with six-symmetrical hexagonal dots are obtained on three areas marked in Figure 1f (including two different domains and their merged region). They are oriented within 78.5 ± 0.2°, indicating that the two merged

domains are aligned with the same direction and there are no dislocations at the

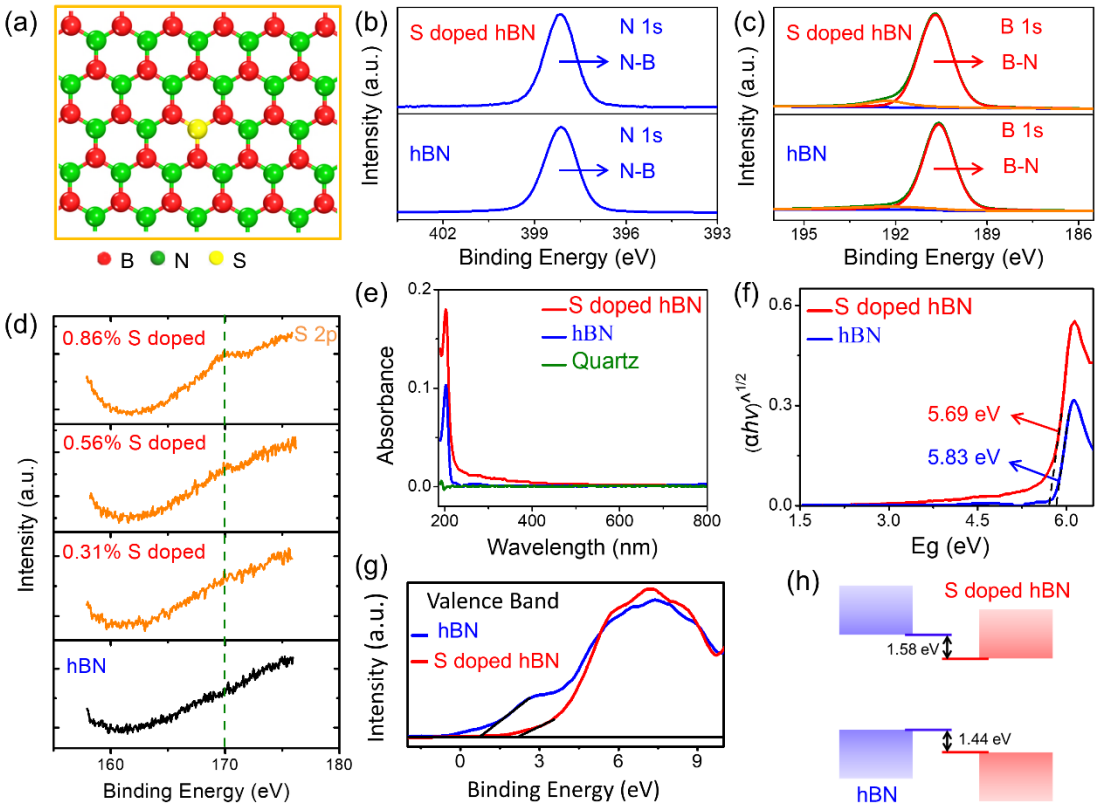

Figure 3. XPS spectra and optical bandgap of hBN and S doped hBN. (a) Schematic illustration of S atoms doped in N sites. (b-d) XPS core level spectra of N 1s, B 1s and S 2p of hBN and S doped hBN. (e, f) Optical absorption spectra and plots of $(\alpha hv)^{1/2}$ versus Eg. (g, h) XPS valence band spectra and band-edge relative position of hBN and S doped hBN.

interface (Figure 1g-i). Corresponding high-resolution TEM images of two merging domains in Figure S4 indicates the high quality. Furthermore, we find that the AFM image is highly sensitive to grain boundaries and wrinkles in the polycrystalline films.[36-38] The image from the atomic force microscope (AFM) shows that there are no grain boundaries or wrinkles within the synthesized sample (Figure S5a). Raman mapping of the E_{2g} (in-plane vibration) phonon peak near 1370 cm^{-1} of the merged region shows a uniformly yellow color, indicating the absence of noticeable defects such as grain boundaries and wrinkles (Figure S5b). Liquid crystals (LC)-assisted polarized optical microscopy (POM) was employed to analyze the lattice orientation of the synthesized hBN monolayer films (Figure S6). There was no particular contrast observed, confirming the formation of wafer-scale S doped hBN monolayer film. To further assess the quality of the stitching between domains, the samples are exposed to H_2 for etching (Figure S7). For H_2 etching, the samples are placed in the center of a quartz tube positioned in a CVD furnace and exposed to the flow of 5 sccm H_2 and 120 sccm Ar for 30 min at 1,000 °C for etching. Edges of the holes marked by the dashed lines in the insets after etching are parallel with each other, which shows that there are no rotation angles between different domains.

The as-grown S doped hBN film is transparent without apparent contrast on Au substrates (Figure 2a). After transferred onto SiO_2/Si substrates, a uniform color contrast between the sample and SiO_2/Si substrate can be observed, demonstrating the successful synthesis of large-area and homogeneous S doped h-BN film on the Au layer (Figure 2b, Figure S8a). The height of S doped hBN film is ~0.7 nm obtained from AFM analysis, which is approximated to that of circular domains, indicating the monolayer nature of the sample (Figure S5a, Figure 2c).[33] The homogeneous monolayer was further confirmed by TEM images (Figure 2d, e). The E_{2g} phonon peak at 1370 cm^{-1} of Raman spectrum of the sample also elucidates its monolayer characteristics (Figure S8b). [39] Corresponding Raman mapping collected at the same area with a unique blue color of E_{2g} peak near 1370 cm^{-1} further demonstrates the homogeneity and high crystal quality of the synthesized S doped hBN monolayer film.[39, 40] To demonstrate the successful incorporation of S atoms, the composition of a hBN monolayer film doped with 0.86% (at. %) S was identified using a high-

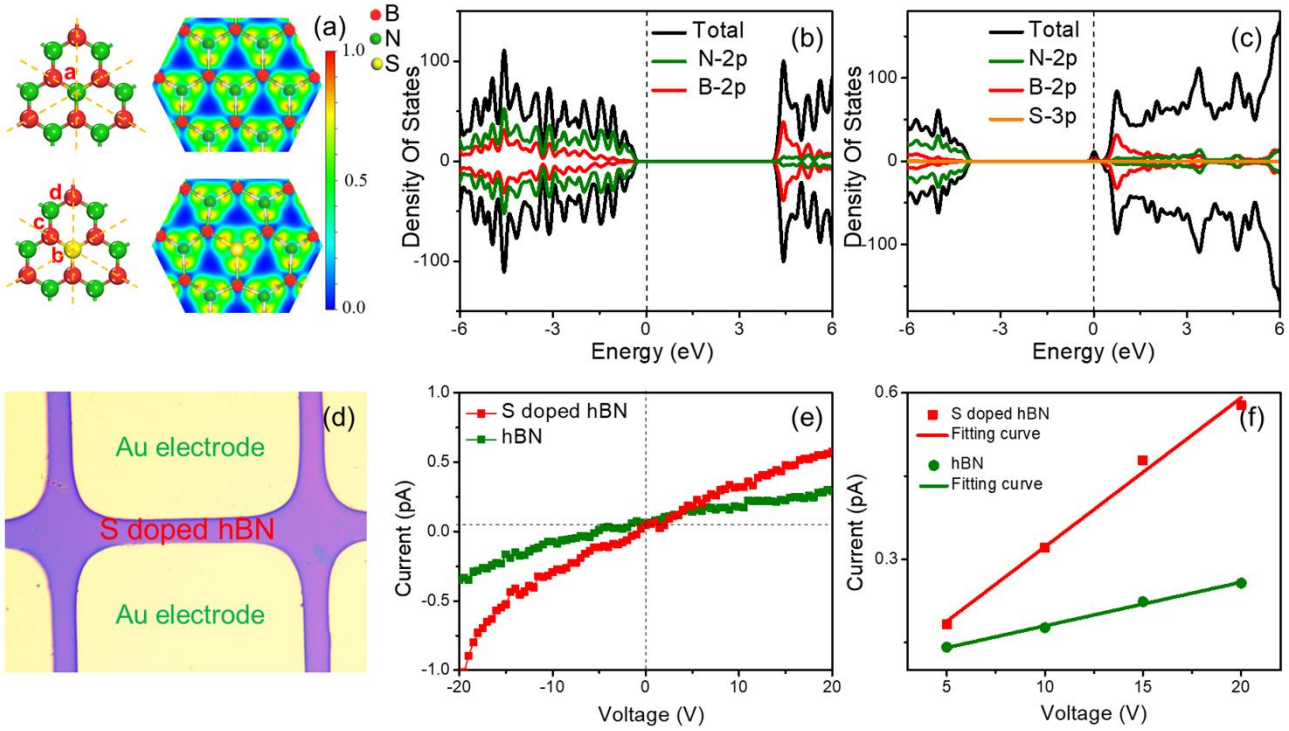

Figure 4. First-principles density functional theory calculations and electrical conductivity properties. (a) The simulated lattice spacings (left) and calculated electron localized functions (ELF, right) of hBN and S doped hBN. (b, c) Density of states of hBN and S doped hBN. (d) OM image of the device structure. (e) Electrical behavior of hBN and S doped hBN. (f) Comparison of electrical conductivity of hBN and S doped hBN, obtained from (e).

angle annular dark-field (HAADF)-scanning transmission electron microscope (STEM) and an energy dispersive spectroscope (EDS) (Figure 2f-i). The EDS mappings of N-K, B-K, and S-K were obtained from the area marked with white rectangle of panel 2f. The results in Figure 2f-I show that the N, B and S atoms are uniformly distributed within the characterized area, indicating the success of S doping in the hBN.

To study the elemental compositions and bonding states of the monolayer films, especially the doping types of S atoms, XPS spectra of N 1s, B 1s and S 2p of hBN and S doped hBN transferred onto SiO_2/Si substrates were analyzed. Survey XPS spectra (Figure S9) and atomic ratios (Table S1) of h-BN films with different S doping concentrations are shown in the supporting information. Figure 3a shows a schematic illustration of the substitutionally doped S atoms in N sites. For both the hBN and S doped hBN, the N1s core level spectra show one characteristic peak with their binding energies of 398.15 eV and 398.18 eV, respectively (Figure 3b). These are attributed to the N-B bonds in the hexagonal lattice, indicating that the N atoms are not bonded with S atoms. The B 1s core level spectrum of hBN is deconvoluted by Gaussian fitting into a main characteristic peak at 190.55 eV (the B-N bond) and a small shoulder peak at 192.25 eV (the B-O bond), which are linked to those from the interactions with SiO_2 substrate and the environmental O_2, respectively (Figure 3c). Whereas for the S doped hBN, the binding energy of B-N is at 190.73 eV, a slightly rightward shift than that of B-N in hBN due to the higher electronegativity of S than that of N, implying changes of bonding states of B after doped with S.[25, 41] It's worth noting that the intensity of shoulder peak at 192.28 eV of S doped hBN is much stronger than that of hBN, indicating that the primarily contribution is from the B-S bond apart from the B-O bond.[25] We further analyzed the XPS core level spectra of S 2p for the S doped hBN. The core level binding energy of S 2p is located at 169.93 eV, and peak intensity is increased with the doping concentration of S (Figure 3d). The deconvolution of XPS core level spectrum of S 2p of 0.86% S doped by Gaussian fitting are shown in figure S10a. This peak is normally attributed to positive charge of S ions (eg. S^{6+}, S^{4+}),[42, 43] whereas some other reports are attributed it to that of S^{2-}.[44, 45] For the synthesis system we used, with a reducing atmosphere of H_2 and a carrier gas of Ar, this peak should be ascribed to S^{2-}, corresponding to the covalence bonds of S-B. It is worth noting that the hexagonal boron nitride unit cell contains a B atom and a N atom, with a total of eight valence electrons. The 2s and $2p_{x,y}$ orbitals of B and N form three planar σ bonds through sp2 hybridization. The nonhybridized pz orbitals of both B and N keep perpendicular to the plane. The lone pair electrons in N pz orbital is assumed to form π bond with the empty pz orbital of B. After S replacing the N atoms, the sp2 hybridized network is still maintained with an extra electron of S in the network. [28] While, if S adopted sp3 hybridization, the generated new bonds should always be present at an even number to balance the overall charge, namely, the S-B

bonds and S-N bonds or other compensating bonds should appear simultaneously. But we only observed S-B bonds, so such a possibility could be excluded.[22]

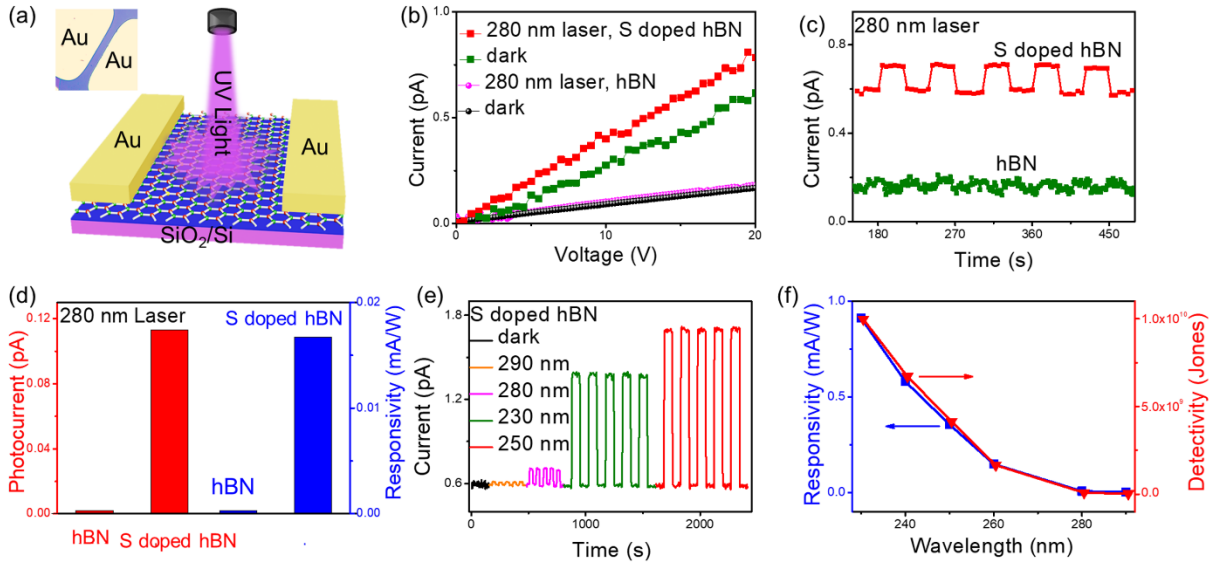

Figure 5. Optoelectronic characteristics of hBN and S doped hBN photodetectors with an extended light response range. (a) Schematic diagram of the device architecture, inset is the OM image of the device. (b) *I–V* curves of hBN and S doped hBN measured in dark and 280 nm light irradiation at 20 V. (c) *I–t* curves of hBN and S doped hBN under 280 nm light irradiation. (d) The column diagram of photocurrent and responsivity of hBN and S doped hBN under 280 nm light irradiation. (e) Stability of S doped hBN under different light wavelength illumination. (f) Responsivity and detectivity of the S doped h-BN photodetector measured under different irradiation wavelengths at 20 V.

The successful growth of S doped hBN monolayer films allows us to study the effect of S doping on their optical properties. To compare the light absorptions and bandgaps of hBN and S doped hBN with 0.86% S, they were transferred onto transparent quartz substrates. The peak absorption of the hBN is located at 202 nm, and its bandgap calculated by the Tauc's formulation is ~5.83 eV, corresponding to the hBN monolayer's absorption characteristics (Figure 3e, f). However, for the S doped hBN, its peak absorption of 202 nm is almost twice as strong as that of the hBN. There is also a weak absorption from 400 nm to 225 nm for the S doped hBN which is different from that of hBN, and its bandgap is narrowed down to ~5.69 eV. The enhanced light absorption and extended light absorption range of the S doped hBN monolayer film will enhance its optoelectronic properties.

X-ray photoelectron valence band (VB) spectra of both the hBN and S doped hBN with varies doping concentrations were collected (Figure S10b). The valence band maxima of the hBN and S doped hBN with 0.86% S were identified to locate at 0.79
eV and 2.23 eV, respectively (Figure 3g). Combined with the valence band maxima and optical bandgaps, their conduction band minima were calculated to be -5.04 eV, and -3.46 eV, respectively. A schematic illustration of the band-edge position is shown in Figure 3h. The obvious changes of band-edge positions with the increase of S doping concentrations are beneficial to construct suitable band-edge alignment of heterostructures for high-performance applications.

To better understand the S substitutional doping sites and their effects on electronic structures, density functional theory (DFT) calculations were performed, more details are in the supporting information. For the hBN, substitution of S in a B site (S_B) and substitution of S in a N site (S_N) are illustrated in Figure S11. The bond lengths of B-N in both the hBN and S doped hBN are 1.450 Å, and those of N-S and B-S for the S doped hBN are 1.732 Å and 1.718 Å, respectively. The bond angles of B-N-B, N-S-N and B-S-B are the same of 120°, indicating that substitutions of S in N sites are more geometrically favorable (Table S2). The formation energies of S atoms substituted in B sites and N sites are 9.34 eV and 7.67 eV, respectively, further elucidating that S atoms are more energetically preferable to be doped in N sites. The calculated results of doping sites are in good agreement with high resolution XPS results.

We then focused on investigating the electronic structures of S doping in N sites. After the S atoms substitutionally doped in the N sites, a threefold symmetry of the hexagonal lattice of hBN is maintained (Figure 4a, left). The electron localization function (ELF) of the B-S covalent bond (~0.78) is similar to that of the B-N covalent bond (~0.80) (Figure 4a, right).[46] For the density of states (DOS) of hBN, the bottom of conduction band (CBM) is mainly constructed by B 2p orbitals, while the top of valence band (VBM) is mainly constructed by N 2p orbitals (Figure 4b). After doping with S, the S 3p orbitals are hybridized with the B 2p orbitals, thus resulting in the formation of new conduction band edge that crosses the Fermi level and

narrows the bandgap (Figure 4c), which is beneficial to improve electrical conductance of the sample. [47]

Our experimental *I-V* results prove that the narrowed bandgap is indeed beneficial to improve the electrical conductivity (Figure 4d-f). To exclude any chemical doping, physical copper mask techniques (details shown in supporting information) were employed to fabricate the measured device electrodes. An optical microscope (OM) image of the device construction is shown in Figure 4d. *I-V* curves for the hBN and S doped hBN shown in Figure 4e are almost symmetric, indicating good contacts between the sample and electrodes.

However, under the same bias voltage, the device constructed by the S doped hBN with 0.86% S exhibits a much higher current than that of hBN due to the enhanced electrical conductance. Comparison of electrical conductivity of hBN and S doped hBN is shown in Figure 4f (values obtained from Figure 4e). The currents of hBN and S doped hBN are both increase with voltages increase, but the S doped hBN has greater increase rate, at a voltage of 20 V increases up to 160.0% after S doping, showing a significant enhancement in the electrical conductivity.

To study the extended wavelength response properties of S doped hBN, we fabricated photodetector devices with a metal-semiconductor-metal (MSM) construction. The working mechanism of a simple photodetector is that photons absorbed in the device generate carriers in the channel, which are then drifted toward electrodes by the applied voltage.[48, 49] Thus, light absorption and conductivity of the sample are two essential factors to affect the photodetector's performance. Figure 5a shows a schematic diagram and an OM image of the photodetector device (inset), which is consisted of two Au electrodes and a 230 μm × 30 μm channel. By irradiating with 280 nm wavelength light, the S doped hBN with 0.86% S shows obvious light induced currents, while the currents of the hBN are almost overlapped with those in the dark environment due to its weak light absorption capability (Figure 5b). Likewise, the time-dependent photo-responses of S doped hBN exhibits stable "on" and "off" characteristics under a periodical light illumination, whereas for the hBN, there are weak responses (Figure 5c). The comparisons of photocurrents and responsivities for both the hBN and S doped hBN are shown in Figure 5d. The photocurrent and responsivity of S doped hBN are ~50 times higher than that of hBN. This significantly enhanced performance is attributed to the improvements of light absorption capability and electrical conductivity of the S doped hBN. Furthermore, after S doping, the samples still have good sensitivities and stable responses to the light irradiation with different wavelengths, indicating the high performance of the synthesized S doped hBN monolayer films (Figure 5e). It shows the maximum current illuminated by the laser at 250 nm rather than at 230 nm, such a disagreement with light absorption is due to the balance between the light absorption and light intensity. However, the highest values of responsivity and detectivity at 230 nm are consistent to the S doped h-BN light absorption, implying that the photo-induced carrier is a bandgap excitation-related process (Figure 5f). The responsivity (~ 1mA/W) of S doped h-BN at 230 nm (0.2 μW/ mm^2) irradiation is comparable to other h-BN photodetectors reported previously, as summarized in Table S3.[14,16,50-52]

CONCLUSIONS

We have systematically studied the optoelectric properties of S doped hBN monolayer films synthesized on a molten Au layer. S atoms doped in the N sites are more geometrically and energetically favorable than those in the B sites. After doped with S atoms, the threefold symmetry of the hexagonal lattice of hBN is still maintained. Whereas the band edge positions are significantly changed, creating a new methodology to construct suitable band-edge alignment heterostructures for high-performance optoelectronic applications. The concentration of S atoms can be precisely adjusted from 0.3% up to 0.9% without deteriorating the crystal quality, which can be potentially used for single-photon emission in quantum information technologies. The hybridization of B 2p states with S 3p narrows the bandgap of S doped hBN, which improves the optoelectronic properties of light absorption and electrical conductivity. The wavelength responses are extended to 280 nm, and the photocurrent and responsivity for light irradiation with a wavelength of 280 nm are ~50 times higher than the pristine hBN. We expect that our new strategy will be beneficial for electronics, optoelectronics, and spintronic technologies.

ASSOCIATED CONTENT

Supporting Information

The Supporting Information is available free of charge at http://pubs.acs.org.

Details of synthesis, additional SEM images, OM images, POM images, EBSD mapping, Raman spectrum and computational details

AUTHOR INFORMATION

Corresponding Author

PingAn Hu – *School of Chemistry and Chemical Engineering, Key Laboratory of Micro-Systems and Micro-Structures Manufacturing of Ministry of Education, State Key Laboratory of Robotics and Systems, Harbin Institute of Technology, Harbin 150080, P. R. China. E-mail: hupa@hit.edu.cn.*

Haiying Xiao – School of Materials Science and Engineering, Harbin Institute of Technology, Harbin, 150080, P. R. China. *E-mail: xhyhit@hit.edu.cn.*

Authors

Biying Tan – *School of Chemistry and Chemical Engineering, Key Laboratory of Micro-Systems and Micro-Structures Manufacturing of Ministry of Education, Harbin Institute of Technology, Harbin 150080, P. R. China.*

You Wu – *School of Chemistry and Chemical Engineering, Key Laboratory of Micro-Systems and Micro-Structures Manufacturing of Ministry of Education, Harbin Institute of Technology, Harbin 150080, P. R. China.*

Feng Gao – *Key Laboratory of Micro-Systems and Micro-Structures Manufacturing of Ministry of Education, Harbin Institute of Technology, Harbin 150080, P. R. China.*

Huihui Yang – *Key Laboratory of Micro-Systems and Micro-Structures Manufacturing of Ministry of Education, Harbin Institute of Technology, Harbin 150080, P. R. China.*

Yunxia Hu – *Key Laboratory of Micro-Systems and Micro-Structures Manufacturing of Ministry of Education, Harbin Institute of Technology, Harbin 150080, P. R. China.*

Huiming Shang – *School of Chemistry and Chemical Engineering, Key Laboratory of Micro-Systems and Micro-Structures Manufacturing of Ministry of Education, Harbin Institute of Technology, Harbin 150080, P. R. China.*

Xin Zhang – *School of Chemistry and Chemical Engineering, Key Laboratory of Micro-Systems and Micro-Structures Manufacturing of Ministry of Education, Harbin Institute of Technology, Harbin 150080, P. R. China.*
Jia Zhang – *Key Laboratory of Micro-Systems and Micro-Structures Manufacturing of Ministry of Education, Harbin Institute of Technology, Harbin 150080, P. R. China.*
Zhonghua Li – *School of Chemistry and Chemical Engineering, Key Laboratory of Micro-Systems and Micro-Structures Manufacturing of Ministry of Education, Harbin Institute of Technology, Harbin 150080, P. R. China.*
YongQing Fu – *Faculty of Engineering & Environment, Northumbria University, Newcastle upon Tyne, NE1 8ST, UK.*
Dechang Jia – *Institute for Advanced Ceramics, School of Materials Science and Engineering, Harbin Institute of Technology, Harbin, 150080, P. R. China.*
Yu Zhou – *Institute for Advanced Ceramics, School of Materials Science and Engineering, Harbin Institute of Technology, Harbin, 150080, P. R. China.*

Notes

The authors declare no competing financial interest.

ACKNOWLEDGMENT

Here, we thank Dr Qing Du of Harbin Institute of Technology for the TEM characterization. This work is supported by National Basic Research Program of China (2019YFB1310200), Foundation for Innovative Research Groups of the National Natural Science Foundation of China (NSFC No. 51521003), Self-Planned Task of State Key Laboratory of Robotics and System (HIT) (no. SKLRS201607B), International Exchange Grant (IEC/NSFC/201078) and Newton Mobility Grant (IE161019) through Royal Society UK and the NSFC.

REFERENCES

(1) Sun, J.; Lu, C.; Song, Y.; Ji, Q.; Song, X.; Li, Q.; Zhang, Y.; Zhang, L.; Kong, J.; Liu, Z., Recent progress in the tailored growth of two-dimensional hexagonal boron nitride via chemical vapour deposition. *Chem. Soc. Rev.* **2018,** *47*, 4242-4257.
(2) Zhang, X.; Zhang, F.; Wang, Y.; Schulman, D. S.; Zhang, T.; Bansal, A.; Alem, N.; Das, S.; Crespi, V. H.; Terrones, M.; Redwing, J. M. Defect-Controlled Nucleation and Orientation of WSe_2 on hBN: A Route to Single-Crystal Epitaxial Monolayers. *ACS Nano*. **2019**, *13*, 3341-3352.
(3) Chilkoor, G.; Jawaharraj, K.; Vemuri, B.; Kutana, A.; Tripathi, M.; Kota, D.; Arif, T.; Filleter, T.; Dalton, A. B.; Yakobson, B. I.; Meyyappan, M.; Rahman, M. M.; Ajayan, P. M.; Gadhamshetty, V. Hexagonal Boron Nitride for Sulfur Corrosion Inhibition. *ACS Nano*. **2020**, *14*, 14809-14819.
(4) Ross, J. S.; Klement, P.; Jones, A. M.; Ghimire, N. J.; Yan, J.; Mandrus, D. G.; Taniguchi, T.; Watanabe, K.; Kitamura, K.; Yao, W.; Cobden, D. H.; Xu, X. Electrically tunable excitonic light-emitting diodes based on monolayer WSe_2 p-n junctions. *Nat. Nanotech*. **2014**, *9*, 268-272.
(5) Huang, W.; Yin, L.; Wang, F.; Cheng, R.; Wang, Z.; Sendeku, M. G.; Wang, J.; Li, N.; Yao, Y.; Yang, X.; Shan, C.; Yang, T.; He, J. Multibit Optoelectronic Memory in Top-Floating-Gated van der Waals Heterostructures. *Adv. Funct. Mater*. **2019**, *29*, 1902890.
(6) Britnell, L.; Gorbachev, R. V.; Jalil, R.; Belle, B. D.; Schedin, F.; Mishchenko, A.; Georgiou, T.; Katsnelson, M. I.; Eaves, L.; Morozov, S. V.; Peres, N. M. R.; Leist, J.; Geim, A. K.; Novoselov, K. S.; Ponomarenko, L. A. Field-Effect Tunneling Transistor Based on Vertical Graphene Heterostructures. *Science* **2012**, *335*, 947-950.
(7) Gao, F.; Chen, H.; Feng, W.; Hu, Y.; Shang, H.; Xu, B.; Zhang, J.; Xu, C. Y.; Hu, P. High-Performance van der Waals Metal-Insulator-Semiconductor Photodetector Optimized with Valence Band Matching. *Adv. Funct. Mater*. **2021**, 2104359.
(8) Mendelson, N.; Chugh, D.; Reimers, J. R.; Cheng, T. S.; Gottscholl, A.; Long, H.; Mellor, C. J.; Zettl, A.; Dyakonov, V.; Beton, P. H.; Novikov, S. V.; Jagadish, C.; Tan, H. H.; Ford, M. J.; Toth, M.; Bradac, C.; Aharonovich, I. Identifying carbon as the source of visible single-photon emission from hexagonal boron nitride. *Nat. Mater.* **2021**, *20*, 321-328.
(9) Shi, Y.; Liang, X.; Yuan, B.; Chen, V.; Li, H.; Hui, F.; Yu, Z.; Yuan, F.; Pop, E.; Wong, H. S. P.; Lanza, M. Electronic synapses made of layered two-dimensional materials. *Nat. Electronics* **2018**, *1*, 458-465.
(10) Ares, P.; Cea, T.; Holwill, M.; Wang, Y. B.; Roldan, R.; Guinea, F.; Andreeva, D. V.; Fumagalli, L.; Novoselov, K. S.; Woods, C. R. Piezoelectricity in Monolayer Hexagonal Boron Nitride. *Adv. Mater.* **2020**, *32*, 1905504.
(11) Dai, S.; Ma, Q.; Andersen, T.; McLeod, A. S.; Fei, Z.; Liu, M. K.; Wagner, M.; Watanabe, K.; Taniguchi, T.; Thiemens, M.; Keilmann, F.; Jarillo-Herrero, P.; Fogler, M. M.; Basov, D. N. Subdiffractional focusing and guiding of polaritonic rays in a natural hyperbolic material. *Nat Commun*. **2015**, *6*, 6963.
(12) Doan, T. C.; Li, J.; Lin, J. Y.; Jiang, H. X. Growth and device processing of hexagonal boron nitride epilayers for thermal neutron and deep ultraviolet detectors. *AIP Advances* **2016**, *6*, 075213.
(13) Zhang, J.; Tan, B. Y.; Zhang, X.; Gao, F.; Hu, Y. X.; Wang, L. F.; Duan, X. M.; Yang, Z. H.; Hu, P. Atomically Thin Hexagonal Boron Nitride and Its Heterostructures. *Adv. Mater*. **2021**, *33*, 2000769.
(14) Sajjad, M.; Jadwisienczak, W. M.; Feng, P. Nanoscale structure study of boron nitride nanosheets and development of a deep-UV photodetector. *Nanoscale* **2014**, *6*, 4577-4582.
(15) Zheng, W.; Lin, R.; Zhang, Z.; Huang, F. Vacuum-Ultraviolet Photodetection in Few-Layered hBN. *ACS Appl. Mater. Interfaces* **2018**, *10*, 27116-27123.
(16) Tan, B. Y.; Yang, H. H.; Hu, Y. X.; Gao, F.; Wang, L. F.; Dai, M. J.; Zhang, S. C.; Shang, H. M.; Chen, H. Y.; Hu, P. A. Synthesis of High-Quality Multilayer Hexagonal Boron Nitride Films on Au Foils for Ultrahigh Rejection Ratio Solar-Blind Photodetection. *ACS Appl. Mater. Interfaces* **2020**, *12*, 28351-28359.
(17) Wang, Y.; Meng, J.; Tian, Y.; Chen, Y.; Wang, G.; Yin, Z.; Jin, P.; You, J.; Wu, J.; Zhang, X. Deep Ultraviolet Photodetectors Based on Carbon-Doped Two-Dimensional Hexagonal Boron Nitride. *ACS Appl. Mater. Interfaces* **2020**, *12*, 27361-27367.
(18) Muchharla, B.; Pathak, A.; Liu, Z.; Song, L.; Jayasekera, T.; Kar, S.; Vajtai, R.; Balicas, L.; Ajayan, P. M.; Talapatra, S.; Ali, N. Tunable electronics in large-area atomic layers of boron-nitrogen-carbon. *Nano Lett.* **2013**, *13*, 3476-3481.
(19) Chen, W.; Li, Y. F.; Yu, G. T.; Li, C. Z.; Zhang, S. B. B.; Zhou, Z.; Chen, Z. F. Hydrogenation: A Simple Approach To Realize Semiconductor-Half-Metal-Metal Transition in Boron Nitride Nanoribbons. *J. Am. Chem. Soc*. **2010**, *132*, 1699-1705.
(20) Zhang, Z.; Zeng, X. C.; Guo, W. Fluorinating Hexagonal Boron Nitride into Diamond-Like Nanofilms with Tunable Band Gap and Ferromagnetism. *J. Am. Chem. Soc*. **2011**, *133*, 14831-14838.
(21) Zhi, C. Y.; Bando, Y.; Terao, T.; Tang, C. C.; Kuwahara, H.; Golberg, D. Chemically activated boron nitride nanotubes. *Chem. Asian J*. **2009**, *4*, 1536-1540.
(22) Weng, Q.; Wang, X.; Wang, X.; Bando, Y.; Golberg, D. Functionalized hexagonal boron nitride nanomaterials: emerging properties and applications. *Chem. Soc. Rev*. **2016**, *45*, 3989-4012.
(23) Fan, M.; Wu, J.; Yuan, J.; Deng, L.; Zhong, N.; He, L.; Cui, J.; Wang, Z.; Behera, S. K.; Zhang, C.; Lai, J.; Jawdat, B. I.; Vajtai, R.; Deb, P.; Huang, Y.; Qian, J.; Yang, J.; Tour, J. M.; Lou, J.; Chu, C. W.; Sun, D.; Ajayan, P. M. Doping Nanoscale Graphene Domains Improves

Magnetism in Hexagonal Boron Nitride. *Adv. Mater*. **2019**, *31*, 1805778.
(24) Weng, Q.; Kvashnin, D. G.; Wang, X.; Cretu, O.; Yang, Y.; Zhou, M.; Zhang, C.; Tang, D. M.; Sorokin, P. B.; Bando, Y.; Golberg, D. Tuning of the Optical, Electronic, and Magnetic Properties of Boron Nitride Nanosheets with Oxygen Doping and Functionalization. *Adv. Mater*. **2017**, *29*, 1700695.
(25) Feng, C.; Tang, L.; Deng, Y.; Zeng, G.; Wang, J.; Liu, Y.; Chen, Z.; Yu, J.; Wang, J. Enhancing optical absorption and charge transfer: Synthesis of S-doped hBN with tunable band structures for metal-free visible-light-driven photocatalysis. *Appl. Catal. B: Environ.* **2019**, *256*, 117827.
(26) Zhao, G.; Wang, A.; He, W.; Xing, Y.; Xu, X. 2D New Nonmetal Photocatalyst of Sulfur‐Doped h‐BN Nanosheeets with High Photocatalytic Activity. *Adv. Mater. Interfaces* **2019**, *6*, 1900062.
(27) Wang, F.; Cao, Y.; Wei, S.; Zhou, Y. Enhanced visible-light response of metal-free doped bulk h-BN as potential efficient photocatalyst: a computational study. *J. Mol. Model.* **2017**, *23*, 23.
(28) Asif, Q. U. A.; Hussain, A.; Nabi, A.; Tayyab, M.; Rafique, H. M. Computational study of X-doped hexagonal boron nitride (h-BN): structural and electronic properties (X = P, S, O, F, Cl). *J. Mol. Model.* **2021**, *27*, 31.
(29) Zhang, Z.; Ji, X.; Shi, J.; Zhou, X.; Zhang, S.; Hou, Y.; Qi, Y.; Fang, Q.; Ji, Q.; Zhang, Y.; Hong, M.; Yang, P.; Liu, X.; Zhang, Q.; Liao, L.; Jin, C.; Liu, Z.; Zhang, Y. Direct Chemical Vapor Deposition Growth and Band-Gap Characterization of MoS_2/hBN van der Waals Heterostructures on Au Foils. *ACS Nano* **2017**, *11*, 4328-4336.
(30) Fu, L.; Sun, Y.; Wu, N.; Mendes, R. G.; Chen, L.; Xu, Z.; Zhang, T.; Rummeli, M. H.; Rellinghaus, B.; Pohl, D.; Zhuang, L.; Fu, L. Direct Growth of MoS_2/hBN Heterostructures via a Sulfide-Resistant Alloy. *ACS Nano* **2016**, *10*, 2063-2070.
(31) Gao, Y.; Liu, Z.; Sun, D. M.; Huang, L.; Ma, L. P.; Yin, L. C.; Ma, T.; Zhang, Z.; Ma, X. L.; Peng, L. M.; Cheng, H. M.; Ren, W. Large-area synthesis of high-quality and uniform monolayer WS_2 on reusable Au foils. *Nat. Commun*. **2015**, *6*, 8569.
(32) Stehle, Y.; Meyer, H. M.; Unocic, R. R.; Kidder, M.; Polizos, G.; Datskos, P. G.; Jackson, R.; Smirnov, S. N.; Vlassiouk, I. V. Synthesis of Hexagonal Boron Nitride Monolayer: Control of Nucleation and Crystal Morphology. *Chem. Mater*. **2015**, *27*, 8041-8047.
(33) Chen, T. A.; Chuu, C. P.; Tseng, C. C.; Wen, C. K.; Wong, H. S. P.; Pan, S. Y.; Li, R. T.; Chao, T. A.; Chueh, W. C.; Zhang, Y. F.; Fu, Q.; Yakobson, B. I.; Chang, W. H.; Li, L. J. Wafer-scale single-crystal hexagonal boron nitride monolayers on Cu (111). *Nature* **2020**, *579*, 219-223.
(34) Wang, L.; Xu, X.; Zhang, L.; Qiao, R.; Wu, M.; Wang, Z.; Zhang, S.; Liang, J.; Zhang, Z.; Zhang, Z.; Chen, W.; Xie, X.; Zong, J.; Shan, Y.; Guo, Y.; Willinger, M.; Wu, H.; Li, Q.; Wang, W.; Gao, P.; Wu, S.; Zhang, Y.; Jiang, Y.; Yu, D.; Wang, E.; Bai, X.; Wang, Z. J.; Ding, F.; Liu, K. Epitaxial growth of a 100-square-centimetre single-crystal hexagonal boron nitride monolayer on copper. *Nature* **2019**, *570*, 91-95.
(35) Lee, J. S.; Choi, S. H.; Yun, S. J.; Kim, Y. I.; Boandoh, S.; Park, J. H.; Shin, B. G.; Ko, H.; Lee, S. H.; Kim, Y. M.; Lee, Y. H.; Kim, K. K.; Kim, S. M. Wafer-scale single-crystal hexagonal boron nitride film via self-collimated grain formation. *Science* **2018**, *362*, 817-821.
(36) Jang, A. R.; Hong, S.; Hyun, C.; Yoon, S. I.; Kim, G.; Jeong, H. Y.; Shin, T. J.; Park, S. O.; Wong, K.; Kwak, S. K.; Park, N.; Yu, K.; Choi, E.; Mishchenko, A.; Withers, F.; Novoselov, K. S.; Lim, H.; Shin, H. S. Wafer-Scale and Wrinkle-Free Epitaxial Growth of Single-Orientated Multilayer Hexagonal Boron Nitride on Sapphire. *Nano Lett*. **2016**, *16*, 3360-3366.
(37) Shi, Y.; Hamsen, C.; Jia, X.; Kim, K. K.; Reina, A.; Hofmann, M.; Hsu, A. L.; Zhang, K.; Li, H.; Juang, Z. Y.; Dresselhaus, M. S.; Li, L. J.; Kong, J. Synthesis of few-layer hexagonal boron nitride thin film by chemical vapor deposition. *Nano Lett*. **2010**, *10*, 4134-4139.
(38) Kim, S. M.; Hsu, A.; Park, M. H.; Chae, S. H.; Yun, S. J.; Lee, J. S.; Cho, D.-H.; Fang, W.; Lee, C.; Palacios, T.; Dresselhaus, M.; Kim, K. K.; Lee, Y. H.; Kong, J. Synthesis of large-area multilayer hexagonal boron nitride for high material performance. *Nat. Commun*. **2015**, *6*.1-11.
(39) Ji, Y.; Calderon, B.; Han, Y.; Cueva, P.; Jungwirth, N. R.; Alsalman, H. A.; Hwang, J.; Fuchs, G. D.; Muller, D. A.; Spencer, M. G. Chemical Vapor Deposition Growth of Large Single-Crystal Mono-, Bi-, Tri-Layer Hexagonal Boron Nitride and Their Interlayer Stacking. *ACS Nano* **2017**, *11*, 12057-12066.
(40) Uchida, Y.; Nakandakari, S.; Kawahara, K.; Yamasaki, S.; Mitsuhara, M.; Ago, H. Controlled Growth of Large-Area Uniform Multilayer Hexagonal Boron Nitride as an Effective 2D Substrate. *ACS Nano* **2018**, *12*, 6236-6244.
(41) Ci, L.; Song, L.; Jin, C.; Jariwala, D.; Wu, D.; Li, Y.; Srivastava, A.; Wang, Z. F.; Storr, K.; Balicas, L.; Liu, F.; Ajayan, P. M. Atomic layers of hybridized boron nitride and graphene domains. *Nat. Mater.* **2010**, *9*, 430-435.
(42) Poh, H. L.; Simek, P.; Sofer, Z.; Pumera, M. Sulfur-doped graphene via thermal exfoliation of graphite oxide in H_2S, SO_2, or CS_2 gas. *ACS Nano* **2013**, *7*, 5262-5272.
(43) Kaur, J.; Malekkhouyan, A.; Selopal, G. S.; Wang, Z. M.; Rosei, F.; Zarrin, H. Bidirectional Superionic Conduction in Surface-Engineered 2D Hexagonal Boron Nitrides. *ACS Appl. Mater. Interfaces* **2021**, *13*, 6532-6544.
(44) Motozaki, W.; Otsuka, T.; Endo, K.; Chong, D. P. Electron binding energies of Si 2p and S 2p for Si- and S-containing substances by DFT calculations using the model molecules. *Polym. J.* **2004**, *36*, 600-606.
(45) Sodhi, R. N. S.; Cavell, R. G. KLL AUGER AND CORE LEVEL (1S AND 2P) PHOTOELECTRON SHIFTS IN A SERIES OF GASEOUS SULFUR-COMPOUNDS. *J. Electron Spectrosc. Relat. Phenom*. **1986**, 41, 1-24.
(46) Yan, Y.; Yang, J.; Du, J.; Zhang, X.; Liu, Y. Y.; Xia, C.; Wei, Z. Cross-Substitution Promoted Ultrawide Bandgap up to 4.5 eV in a 2D Semiconductor: Gallium Thiophosphate. *Adv. Mater.* **2021**, *33*, 2008761.
(47) Gao, H.; Suh, J.; Cao, M. C.; Joe, A. Y.; Mujid, F.; Lee, K. H.; Xie, S.; Poddar, P.; Lee, J. U.; Kang, K.; Kim, P.; Muller, D. A.; Park, J. Tuning Electrical Conductance of MoS_2 Monolayers through Substitutional Doping. *Nano Lett*. **2020**, *20*, 4095-4101.
(48) Huo, N.; Konstantatos, G. Recent Progress and Future Prospects of 2D-Based Photodetectors. *Adv. Mater*. **2018**, *30*, 1801164.
(49) Xie, C.; Lu, X.-T.; Tong, X.-W.; Zhang, Z.-X.; Liang, F.-X.; Liang, L.; Luo, L.-B.; Wu, Y.-C. Recent Progress in Solar-Blind Deep-Ultraviolet Photodetectors Based on Inorganic Ultrawide Bandgap Semiconductors. *Adv. Funct. Mater*. **2019**, *29*, 1806006.
(50) Liu, H.; Meng, J.; Zhang, X.; Chen, Y.; Yin, Z.; Wang, D.; Wang, Y.; You, J.; Gao, M.; Jin, P., High-performance deep ultraviolet photodetectors based on few-layer hexagonal boron nitride. *Nanoscale* **2018**, *10*, 5559-5565.
(51) Gao, M.; Meng, J.; Chen, Y.; Ye, S.; Wang, Y.; Ding, C.; Li, Y.; Yin, Z.; Zeng, X.; You, J.; Jin, P.; Zhang, X., Catalyst-free growth of two-dimensional hexagonal boron nitride few-layers on sapphire for deep ultraviolet photodetectors. *J. Mater. Chem. C* **2019**, *7*, 14999-15006.
(52) Zhou, A. F.; Aldalbahi, A.; Feng, P., Vertical metal-semiconductor-metal deep UV photodetectors based on hexagonal boron nitride nanosheets prepared by laser plasma deposition. *Optical Materials Express* **2016**, *6*, 3286.